Environmental Research 264 (2025) 120286

Contents lists available at ScienceDirect

Environmental Research

journal homepage: www.elsevier.com/locate/envres

Reduced primary productivity and notable resilience of phytoplankton community in the coastal water of southern China under a marine heatwave

Yukun Zhang [a], Guang Gao [a], Huijie Xue [a], Kunshan Gao [a,b,*]

[a] State Key Laboratory of Marine Environmental Science & College of Ocean and Earth Sciences, Xiamen University, Xiamen, China
[b] Co-Innovation Center of Jiangsu Marine Bio-industry Technology, Jiangsu Ocean University, Lianyungang, 222005, China

ARTICLE INFO

Keywords:
Extreme temperature events
The East China Sea
Global warming
Photosynthetic carbon fixation
Phytoplankton community structure

ABSTRACT

Increasing frequency, intensity and duration of marine heatwaves (MHWs) are supposed to affect coastal biological production in different regions to different extents. To understand how MHWs impact coastal primary productivity and community succession of phytoplankton and assess the changes in resilience of phytoplankton communities, we conducted a mesoscale enclosure experiment simulating a MHW in the coastal water of southern China. After 8 days of the MHW (+3 °C) treatment, community biomass was significantly lower than the control's, and primary productivity per volume of water was reduced by about 56%. Nevertheless, the phytoplankton community retrieved its biomass and primary productivity after the temperature was subsequently reset to that of the control. Although the MHW treatment decreased the abundance of diatom and increased the percentages of *Synechococcus* and Prasinophytes, the main phytoplankton functional types showed positive resilience that allowed the recovery of the phytoplankton community after the MHW. Our results indicate that key phytoplankton functional types in the southern coastal waters of China exhibited significant resilience, recovery, and temporal stability under the influence of the marine MHW by 3 °C rise. However, reduced primary productivity during the MHW period, along with decreased biomass density, might significantly influence secondary producers. In addition, the altered phytoplankton community structure may affect coastal food web processes at least during the MHW period.

1. Introduction

Progressive ocean warming is concurrent with global warming due to anthropogenic emissions of greenhouse gases (Kweku et al., 2018). One of the notable consequences of global and ocean warming is an increased frequency of Marine Heat waves (MHWs), which have garnered increasing attention due to their impacts on marine ecosystems and sea-farming industries (Frolicher et al., 2018; Laufkötter et al., 2020; Monteiro et al., 2023). MHWs have been defined as periods when daily sea surface temperature (SST) exceeds the 90 % threshold of a 30-year historical baseline for over five days (Hobday et al., 2016). The MHWs can cover areas spanning regions up to thousands of square kilometers (Masson-Delmotte et al., 2021), with increased frequency, duration, extent and intensity along with exasperating global warming (Oliver et al., 2018, 2021). In recent decades, MHWs have been documented in the North Atlantic and North Pacific (Scannell et al., 2016), Northeast Pacific (Cheung and Frölicher, 2020), the Mediterranean Sea (Garrabou et al., 2022), the Arabian Sea (Chatterjee et al., 2022), Bering Sea (Carvalho et al., 2021), Australian waters (Perkins-Kirkpatrick et al., 2016), Arctic Ocean (Hu et al., 2020), even in the Chinese waters (Wu et al., 2012), including the South China Sea (Yao and Wang, 2021), the East China Sea (Tan et al., 2023), the Yellow Sea (Li et al., 2022) and the Bohai Sea (Yao et al., 2020).

Phytoplankton, the main primary producer, supply energy via photosynthesis to marine ecosystems, supporting diverse marine lives and contributing to nearly half of the global primary productivity (Sakshaug et al., 2009; Vallina et al., 2014). However, many phytoplankton species are supposed to be vulnerable to MHWs, which impact their physiology and community stability (Gao et al., 2021; Smale et al., 2019; Smith et al., 2023), and have been considered accountable for the morbidity and mortality of shellfish and outbreaks of harmful algal blooms (Roberts et al., 2019). Anomalous warming of water temperatures along the west coast of North America in the spring of 2015 led to an outbreak of the toxic diatom *Pseudo-nitzschia*, which secretes the neurotoxin chondrocyanobacterial acid that was detected in many stranded mammals and affected the coastal razor clam, rock crab, and

* Corresponding author. State Key Laboratory of Marine Environmental Science & College of Ocean and Earth Sciences, Xiamen University, Xiamen, China.
E-mail address: ksgao@xmu.edu.cn (K. Gao).

https://doi.org/10.1016/j.envres.2024.120286
Received 3 September 2024; Received in revised form 31 October 2024; Accepted 1 November 2024
Available online 2 November 2024

Dungeness crab fisheries (McCabe et al., 2016). The MHWs that occurred in Australia in 2015–2016 disrupted the symbiotic relationship between corals and the microalgal symbiodinium, leading to coral bleaching (Hughes et al., 2017). From July to August 2022, stony coral communities in the China Grand Bay area in the northern part of the South China Sea experienced an unprecedented bleaching event due to an encroaching MHW (Mo et al., 2022).

The China Sea, located at the intersection of the East Asian continental shelf and the Western Pacific continental shelf, is one of the largest shelf seas in the world, providing ecological services and useful biological resources (Li, 1984). Because of its proximity to land and the fact that most of the sea is less than 200 m deep, it is highly vulnerable to human activities and climate change (Li, 1984; Wong et al., 2015). In the East China Sea, the rate of ocean warming is significantly faster than the global average, therefore, it is suggested that the Chinese marine ecosystems would be more susceptible to MHWs (Wu et al., 2012). In the Chinese coastal waters, an extensive fishery industry relies on the sustainability of primary production. Therefore, understanding how MHWs affect the physiology and primary production of the phytoplankton community in these waters is of general interest. Although there have been literatures documenting MHWs and exploring their causes (Holbrook et al., 2019; Laufkötter et al., 2020; Sen Gupta et al., 2020), little has been documented on their impacts on phytoplankton physiology and ecology, especially in the Chinese waters. In the Mediterranean Sea, MHWs significantly promoted gross primary production, community respiration, and phytoplankton growth and altered the phytoplankton community (Soulie et al., 2023; Soulié et al., 2022).

Since different regions have distinct traits of chemical and physical environments with specific conditions that govern the biogeochemical and ecological processes, MHWs in different waters may give rise to impacts of different extents or directions in different waters. This study conducted a land-based mesoscale enclosure experiment off the coast of southern China. The objective of this work was to investigate how the MHW affects the primary productivity, community composition, and physiological changes of phytoplankton assemblages in this region and to provide a regional examination of primary production in the context of global ocean climate changes. The data obtained from the experiments were used to quantify the resistance, recovery, resilience and temporal stability of the phytoplankton functional types. We found that MHW up to +3 °C for 8 days reduced the primary productivity, but the phytoplankton assemblages exhibited a notable resilience in terms of their physiological performance and community stability.

2. Materials and methods

2.1. Mesocosm Setup

In order to investigate the impact of marine heatwaves (MHWs) on coastal phytoplankton communities, mesoscale enclosure experiments were conducted from March 3 to 20, 2023, at the Dongshan Swire Marine Station (D-SMART) of Xiamen University. The culture systems were water-jacketed cylinders made of polymethyl methacrylate with an inner barrel capacity of approximately 30 L (Supplementary Fig. 1). The culture temperature of the inner part is controlled by circulated water through the jacketed surrounding layer. Before the experiment, the water collection equipment and the inner barrel of the cylinders were soaked with 0.1N hydrochloric acid for more than 12 h and then washed with tap water and ultra-pure water.

The experiment was carried out with two groups, namely the control and the MHW group, and each group had three repetitive culture systems (Supplementary Fig. 1). At the beginning of the experiment, natural seawater collected from the D-SMART nearshore was filtered through a 200 μm sieve silk (removing large zooplankton) into a 100 L white bucket, from which the seawater was simultaneously run into the six culture systems. Ambient air was bubbled into the culture system at a flow rate of 500 ml min^{-1}. From days 1–9 of the experiment, the temperature of the control group was maintained at about 20 °C (similar to that *in situ*), while the temperature of the MHW group was controlled at about 23 °C. From days 9–17, the temperature of the MHW group was reduced and remained consistent with that of the control group.

2.2. Determination of environmental parameters

The solar radiation data was obtained with real-time monitoring equipment (EKO, Japan) installed on the D-SMART roof, which instantly monitors and records averages per minute of the intensity of solar radiation. The temperature was measured manually with a digital thermometer (PAMPAS, China) at 12:30 daily, repeated three times for each culture system, and averaged. The pH values of the culture systems were measured in the afternoon by a pH meter (Orion Star A211, Thermo Scientific), which was calibrated with a NIST-traceable pH buffer. The total alkalinity (TA) was determined by acid-base titration (Lewis and Wallace, 1998), and calculated according to the equations in the supplementary information.

2.3. Determination of macronutrients

The seawater samples for nutrient determination were filtered through a cellulose acetate filter membrane with a pore size of 0.45 μm. Subsequently, 15 ml of the filtrate was aliquoted into a 50 ml high-density polyethylene bottle and promptly frozen at −20 °C for later determination of NO_2^-, NO_3^-, and PO_4^{3-}. An additional 15 ml and 25 ml of the filtrate were collected, and chloroform was introduced to achieve a final concentration of 1‰, then stored at 4 °C and −20 °C, respectively, for subsequent measurements of the SiO_3^{2-} and NH_4^+ concentrations. The concentrations of NO_2^-, NO_3^-, PO_4^{3-}, and SiO_3^{2-} were measured using an auto-analyzer (AA3, Seal, Germany) at room temperature. The concentration of NH_4^+ was detected spectrophotometrically using indophenol blue at 25 °C.

2.4. Chlorophyll a and carotenoid measurement

The collected culture seawater of 200 ml was filtered onto the 25-mm-diameter Whatman GF/F filters by a low-pressure vacuum pump (<0.02 Mpa). Then, the filters were placed into a 15 ml centrifuge tube in darkness at 4 °C for 12 h after 5 ml of pure methanol was added. The extract was centrifuged at 8000 rpm at 4 °C for 15 min. Finally, a UV spectrophotometer (UV-1800, Japan) was used to measure the absorbance values of the supernatant at wavelengths of 750, 665, 652, 510, and 480, and the concentrations of chlorophyll *a* (Chl *a*) and carotenoid were calculated. (Ritchie, 2006).

2.5. Phytoplankton community structure

High-performance liquid chromatography is used to analyze changes in phytoplankton community structure by determining the concentrations of representative pigments (Wang et al., 2015). In brief, 200 ml culture seawater was filtered onto the filter membrane (25 mm, Whatman GF/F, USA), then immediately frozen in liquid nitrogen and transferred to a −80 °C ultra-low temperature refrigerator. Before the determination, the filter was placed in a 2 ml brown centrifuge tube, 1 ml of *N, N*-dimethylformamide was added and was placed under −20 °C for 1 h to extract the pigments, during which the mixture was shaken every 20 min. It was then filtered through a 0.22 μm syringe filter to remove debris from the extract solution and mixed with ammonium acetate in a ratio of 1:1 by volume. The mixed solution of 400 μl was injected into high-performance liquid chromatography (Shimadzu, Japan) equipped with a 3.5 μm Eclipse XDB C8 column (4.6 × 100 mm, Agilent Technologies), and a binary gradient solvent system was used. Pigments were discerned through chromatography employing genuine standards from DHI, Denmark, and diode-array spectroscopy covering a wavelength range of 300–800 nm. The relative contributions of nine

phytoplankton groups to the total Chl *a* were assessed by employing the CHEMTAX program, which utilized 13 selected abbreviated pigments for calculation (Xiao et al., 2018).

2.6. Measurements of primary productivity

$NaH^{14}CO_3$ was spiked in the sampled water to estimate the primary productivity of the phytoplankton assemblages in the cultures. Before sunrise, about 50 ml of seawater from each culture system was sampled into a 50 ml quartz tube, and then 5 μCi $NaH^{14}CO_3$ was added before tightening the tube cap to block gas exchange. The quartz tubes were fixed in a constant temperature water tank at 20 °C or 23 °C and exposed to the full spectrum of solar radiation (in the presence of UV irradiances as in the surface seawater). After sunset, the water sample was filtered with a glass cellulose membrane (25 mm, Whatman GF/F, USA) in a low-light environment to collect the ^{14}C-labeled photosynthetic cells and then immediately stored at −20 °C until measurement. Prior to the measurements, the GF/F membranes were unfolded and placed at the bottom of liquid scintillation vials (20 ml), then fumigated with the concentration of 12 N hydrochloric acid for 12 h and were subsequently dried at 60 °C to remove unfixed inorganic ^{14}C. Subsequently, 5 ml of scintillation solution (Hisafe 3, PerkinElmer, USA) was added to the liquid scintillation vials to react for 2 h and then measured. Sample counts per minute (CPM) were determined using a Liquid Scintillation Counter (LS 6500, Beckman Coulter, USA). The rates of photosynthetic carbon fixation were calculated as previously described (Gao et al., 2007).

2.7. Determination of chlorophyll fluorescence parameters

In this experiment, chlorophyll fluorescence parameters of the phytoplankton community in the mesocosms were determined on days 9 (end of the MHW treatment) and 17. Photosystem II (PSII) effective photochemical efficiency (Yield) and non-photochemical quenching (NPQ) were measured by the In-Situ FIRe (In-Situ Fluorescence Induction and Relaxation system, Satlantic, NS Canada). The saturation pulse was set to 5×10^4 μmol photons m^{-2} s^{-1} (80 μs). NPQ was calculated as NPQ = Fm/Fm' −1 (Genty et al., 1989), where Fm is the maximum fluorescence measured before sunrise (6:00), and the apparent maximal fluorescence, Fm', was measured at 10:30, 12:30, 15:00, and 18:30.

2.8. Resistance, resilience, recovery, and temporal stability estimates

The data obtained from the experiments were used to quantify resistance, resilience, recovery and temporal stability of the phytoplankton community (Table 1 and Supplementary Table 1) based on function stability (biomass production and daytime primary productivity) and compositional stability (key phytoplankton functional groups). These parameters were estimated according to the definitions by (Hillebrand et al., 2018). In brief, the log response ratios (LRR) of the MHW group relative to that of the control group were assessed for each day. Resistance (a) was expressed as the ability to withstand the disturbance based on the changes of LRR. Resilience (b) was the slope of the linear function fitted to the LRR values from D9 to D17 (the period after MHW), reflecting the tempo of recovery following the MHW treatment. Recovery (c) was estimated as the LRR on the experiment's last day (D17) to assess the degree of function or compositional restoration at the end of the experiment. The temporal stability (d) was determined by taking the inverse of the standard deviation of the residuals around resilience (Hillebrand et al., 2018). All data for the same variable (e.g., Chl *a*, carotenoid, etc.), as well as three single sets of data, were fitted to a composite linear relationship and three independent linear relationships, respectively, resulting in one composite slop (b) value and three independent slop values, and then the residuals of these three independent estimates and the corresponding composite value were computed separately. The estimation formulae using the relevant data from D9-D17 and the corresponding interpretations are given in Table 1, and the linear fitting of the LRR for D9-D17 was achieved by using Origin 2021 software.

Table 1
| Stability parameters estimated and the experimental periods that they are calculated for, as well as their interpretation. The definition of stability parameters was referred to (Hillebrand et al., 2018; Soulié et al., 2022).

Parameter	Period	Estimation	Interpretation
Resistance (a)	D9	$a = \ln\left(\frac{X_{MHW}}{X_C}\right)$	a = 0, maximum resistance a >0, over-performance a <0, underperformance
Resilience (b)	D9-17	$\ln\left(\frac{X_{MHW}}{X_C}\right) = b^* t + i$	b = 0, no recovery b > 0, faster recovery (if i < 0) b < 0, further deviation from control (if i < 0)
Recovery (c)	D17	$c = \ln\left(\frac{X_{MHW}}{X_C}\right)$	c = 0, maximum recovery c > 0, overcompensation c < 0, incomplete recovery
Temporal stability (d)	D9-17	$d = \frac{1}{(sd(res_b))}$	The larger the *d* value the lower fluctuation

X_C and X_{HW} represent the investigated data for quantifying the functional stability and compositional stability in the control and heatwave groups, respectively. The intercept i indicates the direction of the response to the heatwaves (i > 0, the parameter was higher in the HW treatment than in the control; i < 0, the parameter was lower).

3. Data analysis

Each group in the experiment had three independent biological replicates, so all data were presented as mean ± standard deviation (n = 3). For each day's data on pigment and chlorophyll fluorescence parameters, a one-way analysis of variance was used to test whether there was a significant difference between the two groups (Control and MHW) on that day ($p < 0.05$). For photosynthetic carbon fixation data, after testing for significant differences between treatments, the least squared difference (LSD) was used to compare differences between the groups ($p < 0.05$).

4. Results

4.1. Changes in physical and chemical parameters

The weather was clear and sunny on most days during the experimental period (March 3 to 20, 2023). The solar photosynthetically active radiation (PAR) fluctuated, with daytime averages ranged 674–980 μmol photons m^{-2} s^{-1} from day 1 to day 14. On the 15th day, it was rainy, and the average PAR dropped to the lowest value of 251 μmol photons m^{-2} s^{-1}. Over the final three days, commencing from the 15th day of the experiment, the average PAR demonstrated a consistent upward trajectory and reached 573 μmol photons m^{-2} s^{-1} on the last day (Fig. 1A). The temperature within the culture system was relatively stable throughout the experimental period. In the control group, it fluctuated between 18.8 and 21.2 °C during the first 9 days, while in the MHW group, it varied within the range of 22.1 – 23.7 °C. Since day 9, the temperature for both groups fluctuated between 19.8 and 21.4 °C (Fig. 1B).

Throughout the experiment, pH and DIC changed dramatically in both the control and MHW groups, but with similar trends between the two groups (Fig. 1C and D). The pH on day 5 was significantly different between the two groups (7.99 ± 0.01 in the control group and 8.35 ± 0.01 in the MHW group) due to the blooming of phytoplankton. The levels of pH and DIC at all other times did not differ significantly. The pH values of the control and MHW groups increased from 8.06 ± 0.01 and 8.03 ± 0.01 to a maximum of 8.43 ± 0.01 and 8.49 ± 0.02 till day 7, respectively. It gradually decreased from day 7 to day 17 to about 8.12 in both groups (Fig. 1C). The DIC concentration showed the opposite

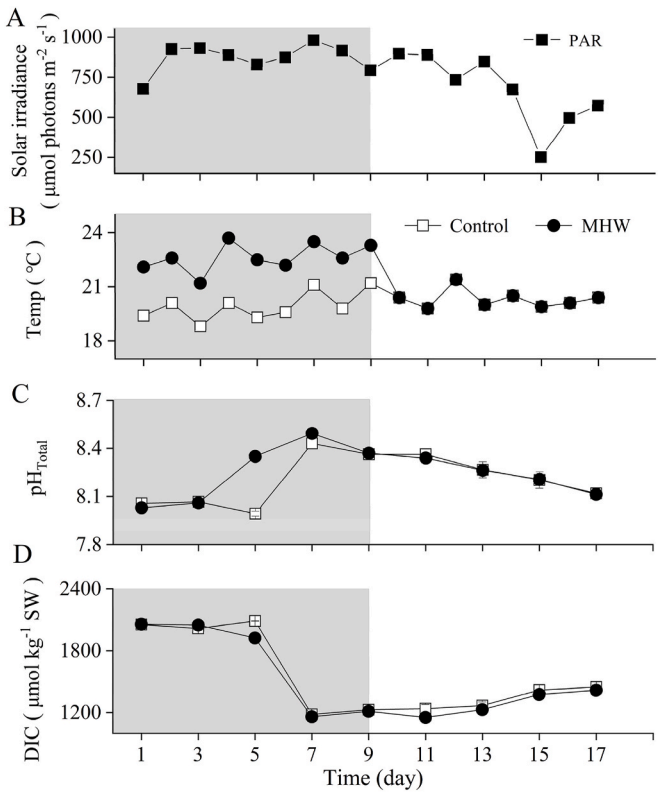

Fig. 1. | Changes of **(A)** solar photosynthetically active radiation (PAR), **(B)** water temperature, **(C)** pH_{Total} and **(D)** DIC during the mesocosm experiment. The shaded parts indicate the duration of the heatwave treatment. Data are means ± SD of three replicates for the control (open square) and heatwave groups (solid circle).

changes to that of pH, decreasing and then increasing. The concentration of DIC in control and MHW groups changed from the initial value of 2063.83 ± 16.03 μmol kg^{-1} to 2089.71 ± 2.10 μmol kg^{-1} and 1924.48 ± 8.14 μmol kg^{-1} on day 5, and then to the lowest levels of 1182.92 ± 11.91 μmol kg^{-1} and 1160.44 ± 23.36 μmol kg^{-1} on day 7, respectively. It increased from day 7 to day 17 to 1448.25 ± 22.22 μmol kg^{-1} and 1417.26 ± 13.16 μmol kg^{-1}, respectively, for the control and MHW groups (Fig. 1D).

The initial concentrations of NO_3^-, PO_4^{3-}, $Si(OH)_4$, and NH_4^+ were 16.56 ± 2.07 μmol L^{-1}, 0.94 ± 0.12 μmol L^{-1}, 28.63 ± 0.10 μmol L^{-1}, and 0.64 ± 0.14 μmol L^{-1}, respectively. The concentrations of NO_3^-, PO_4^{3-}, and $Si(OH)_4$ in the control group remained relatively stable for the first 3 days, followed by a steep decline to a depleted state from day 3 to day 9 until the end of the experiment. In the MHW group, these concentrations mirrored that of the control group during the first 9 days, with levels being lower than that of the control group (Fig. 2). The concentration of PO_4^{3-} became depleted since day 5 and day 9 in MHW and control group respectively (Fig. 2B). However, the concentration of NO_3^- in the MHW group (9.431 ± 1.54 μmol L^{-1}) increased by about 11-fold compared to the control (0.84 ± 0.90 μmol L^{-1}) on the 11th day, then slowly decreased to a state of depletion at the end of the experiment (Fig. 2A). The $Si(OH)_4$ also increased on the 11th day and maintained a concentration between 27.42 ± 3.58 μmol L^{-1} to 32.57 ± 3.77 μmol L^{-1} during the 11th to 17th day (Fig. 2C). The concentration of NH_4^+ in the two groups showed a fluctuating trend with no obvious changes, with that of the MHW group higher than that of the control group (Fig. 2D).

4.2. Changes in chlorophyll a and carotenoid concentrations

The concentrations of chlorophyll *a* (Chl *a*) and carotenoid (Fig. 3) increased rapidly and then declined, with the peaks being higher and

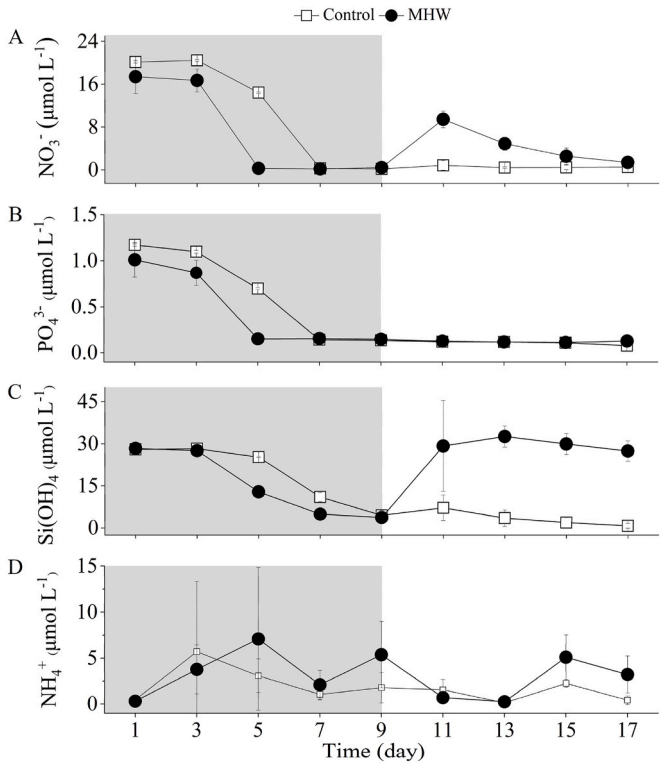

Fig. 2. | Temporal changes of the nutrient concentrations in the control (open square) and heatwave groups (solid circle) during the mesocosm experiment. **(A)** NO_3^-, **(B)** PO_4^{3-}, **(C)** $Si(OH)_4$ and **(D)** NH_4^+. The shaded part is the duration of the heatwave treatment. Data are means ± SD of three replicates.

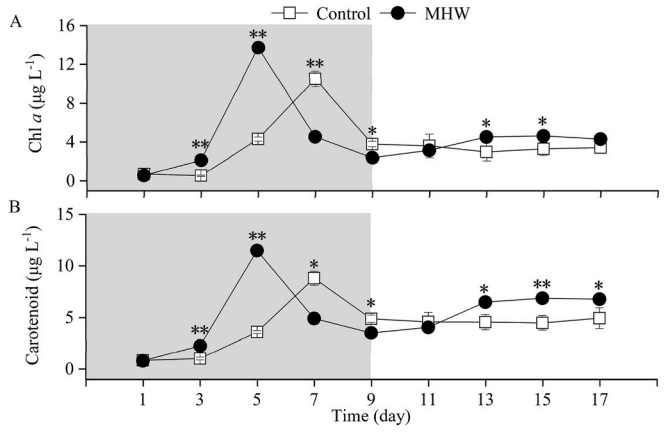

Fig. 3. | Temporal changes of chlorophyll *a* and carotenoids in control (open square) and heatwave groups (solid circle) during the mesocosm experiment. **(A)** Chlorophyll *a*, **(B)** carotenoids. The shaded part is the duration of the heatwave treatment. Data are means ± SD of three replicates. The symbols * and ** denote significant differences at the same time point between the control and HW groups at $p < 0.05$ and $p < 0.01$, respectively (one-way ANOVA).

appearing earlier by 2 days in the MHW treatments. In the control group, the Chl *a* concentration rapidly increased from 0.71 ± 0.10 μg L^{-1} on day 1 to 10.52 ± 0.79 μg L^{-1} on day 7 at the apex, then dropped to 3.79 ± 0.27 μg L^{-1} on day 9 and stabilized between 2.98 ± 0.92 μg L^{-1} to 3.61 ± 1.21 μg L^{-1} on days 11–17 (Fig. 3A). The concentration of carotenoid exhibited a rapid surge from 0.84 ± 0.03 μg L^{-1} on day 1 to 8.81 ± 0.68 μg L^{-1} on day 7, reaching its peak. Subsequently, it declined to 4.88 ± 0.36 μg L^{-1} on day 9 and remained relatively stable to day 17 (Fig. 3B). In the MHW group, the Chl *a* concentration was 0.56 ± 0.07 μg

L^{-1} at the beginning, increased by about 24.5 fold (13.73 ± 0.31 μg L^{-1}) to reach its peak on day 5, then rapidly decreased to2.39 ± 0.29 μg L^{-1} on day 9. From day 9 to day 13, it gradually increased to 4.51 ± 0.23 μg L^{-1} and remained within the range of 4.29 ± 0.36 μg L^{-1} to 4.62 ± 0.26 μg L^{-1} until the end of the experiment and were 1.25–1.51 fold of that of the control group on day13 - day17 (Fig. 3A). Carotenoid concentration in the MHW groups showed a similar pattern but increased by 1.4–1.5 fold at day 13–17 after the temperature was reset to the control level (Fig. 3B).

4.3. Primary productivity

The initial day-time primary productivity of the phytoplankton assemblages was 12.04 ± 3.50 μg C L^{-1}. During the meso-incubations, it increased with time to 142.69 ± 18.77 μg C L^{-1} at day 9 and then declined to 129.75 ± 11.59 μg C L^{-1} at day 17 in the control. The MHW treatment led to decreased primary productivity by about 56% at day 9 (end of the MHW treatment) and increased by about 40% at day 17 after the temperature had been reset to that of the control for a week, compared to that of the control (Fig. 4A). The chlorophyll *a*-based photosynthetic C fixation also increased from the initial 18.15 ± 3.33 μg C (μg Chl *a*)$^{-1}$ to 37.72 ± 5.05 μg C (μg Chl *a*)$^{-1}$ at day 9, and then increased to 38.97 ± 10.13 μg C (μg Chl *a*)$^{-1}$ at day 17. The MHW treatment also first reduced and then increased the rate but then led to insignificant changes compared to that of the control (Fig. 4B).

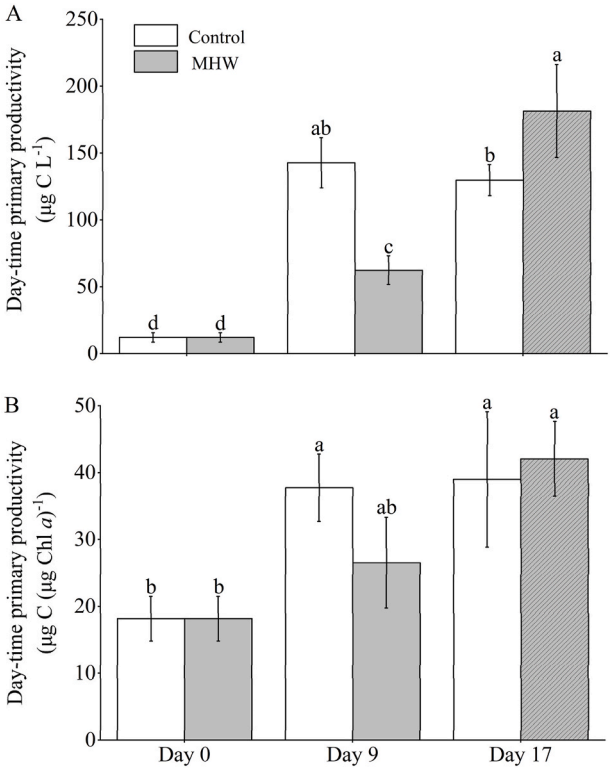

Fig. 4. | Changes in day-time primary productivity in the control and heatwave groups on days 1, day 9 (end of HW treatment) and day 17 (end of the experiment). **(A)** Day-time primary productivity per volume of water, **(B)** day-time photosynthetic carbon fixation per chlorophyll *a*. The white columns indicate the control group, the gray columns indicate the heatwave treatment periods (D1 and D9, without slashes) and the post-MHW (D17, with slashes). Having different letters above the columns indicates significant differences, and having the same letters indicates no significant difference. ($p < 0.05$, one-way ANOVA). Data are means ± SD of three replicates.

4.4. Chlorophyll fluorescence parameters

The photochemical parameter, the effective quantum yield, showed a typical diurnal pattern opposite to that of solar radiation, showing the minimum at midday and the maximal values during twilight periods (Fig. 5A and B). The yield values of day 9 were similar in the control and MHW groups (Fig. 5A). However, the yield of the MHW groups at day 17 was 1.60, 1.29 and 1.28 times that of the control group at 10:30, 12:30 and 15:30, respectively (Fig. 5B, $p < 0.05$). The non-photochemical quenching (NPQ, an indicator for high light stress) was higher in the control group than in the MHW group throughout the day at day 9. In contrast, at day 17 (Fig. 5C and D), the MHW treatment decreased NPQ by 20%, but the post-MHW effect gave rise to an increase of NPQ by 21%, compared to that of the control at 12:30 (Fig. 5D, $p < 0.05$).

4.5. Phytoplankton community composition and succession

The phytoplankton in the coastal waters consisted of five principal groups, with diatoms accounting for about 50% of the total, cryptophytes for about 20%, prasinophytes for about 14%, and chlorophytes and *Synechococcus* for about 8% each (Fig. 6A). The phytoplankton composition changed drastically after 9 days of incubation, with 80%, 6%, 5%, 4%, and 6% of the above five phytoplankton taxa in the control group. In the MHW group, however, the proportions were correspondingly 70%, 4%, 7%, 6% and 12% (Fig. 6B). At the end of the experiment (day 17), the percentages of the five phytoplankton taxa were 78%, 3%, 5%, 4%, and 9% in the control, and 70%, 3%, 10%, 5%, and 11% in the MHW group (Fig. 6C). While the diatom percentage increased either in the control or the MHW treatment during the incubations, the prior MHW treatment appeared to have reduced its abundance after the temperature had been reset to that of the control for a week.

Graphing the changes in total chlorophyll *a* (TChl *a*) and the five main phytoplankton groups over incubation time allows for more visual analysis of changes in the composition of the phytoplankton community (Supplementary Fig. 2). The total Chl *a* concentration trend in the culture system determined and analyzed by HPLC with incubation time was the same as that analyzed by Chl *a* determination by UV spectrophotometry using pure methanol extraction (Fig. 3a and Supplementary Fig. 2A). The abundance of the above five phytoplankton groups increased and then decreased with time. In the MHW group, the biomass of all five phytoplankton groups reached the highest value at day 5 and was higher than that of the control group. In the control group, Cryptophytes, Prasinophytes, and Chlorophytes also reached the highest value at day 5, while diatom and *Synechococcus* reached the highest value at day 7. Overall, there was an inflection point from day 5 to day 7, with the biomass in the MHW groups being higher than that of the control. At the end of the incubation at day 17, diatom biomass was slightly higher in the control than in the MHW group, while that of Synechococcus, Chlorophytes, and Prasinophytes biomass in the MHW group exceeded that of the control, and the percentage of Cryptophytes was more or less equal between the two groups.

4.6. Functional stability

The functional stability parameters evaluated (Table 1, Supplementary Table 1) indicate that primary productivity and the main phytoplankton functional types were significantly resilient to the impact of the MHW treatment. The estimated resistance value of Chl *a* was −0.46 (<0), indicating that initial heatwave disturbance negatively affects the biomass in the mesocosms. The resilience and recovery of DPP (day-time primary productivity) and Chl *a* were 0.06 and 0.09, 0.09 and 0.23, respectively, indicating relatively rapid and positive recovery after the heatwave treatment. During the recovery phase (post-MHW), the changes in DPP and Chl *a* fluctuated less, and the overall trend was stable (Temporal stability values are 95.25 and 95.27). For compositional stability, all five phytoplankton functional types (PFTs) showed

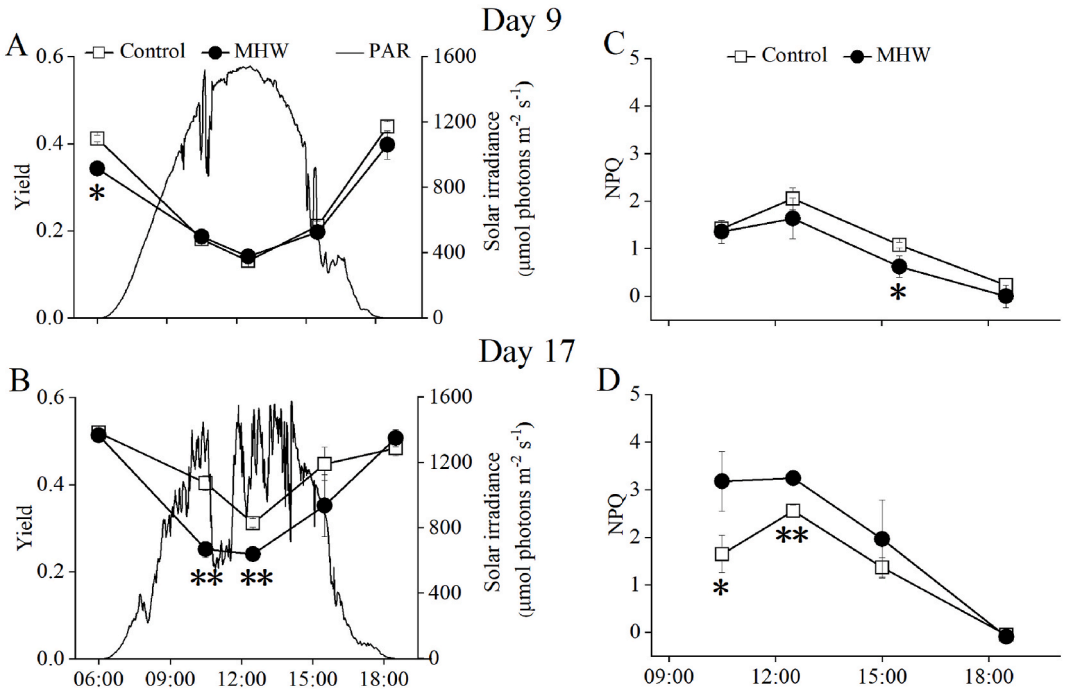

Fig. 5. | Diurnal changes in PSII quantum yield (Yield) and the non-photochemical quenching (NPQ) of phytoplankton assemblages grown under control (open square) and HW groups (solid circle) at days 9 and 17, respectively. **(A, B)** Effective PSII quantum yield and **(C, D)** Non-photochemical quenching (NPQ). Data are means ± SD of three replicates. The symbols * and ** denote significant differences of $p < 0.05$ and $p < 0.01$, respectively, between the two data sets at the same time point (one-way ANOVA).

notable resistance (Resistance <0), with Cryptophytes being the maximum deviation from baseline (−1.40) and relatively least resistance and *Synechococcus* being the closest to baseline (−0.26) and relatively more resistant. During the recovery period (days 9–17), all five PFTs recovered faster (>0), with Cryptophyta having the fastest recovery with the largest recovery value (0.21) and *Synechococcus* having the slowest recovery value (0.07). While the diatoms had a negative value (−0.10), the recovery of the other four PFTs was all greater than 0. The largest value was found for Prasinophytes (0.68), and the estimated values for Chlorophytes, Cryptophytes and Synechococcus were 0.22, 0.20 and 0.26, respectively. Based on the interpretations (Table 1), the five PFTs were ranked in the following order in terms of stability during the recovery: *Synechococcus* (97.59) > Diatoms (89.03) > Chlorophytes (85.81) > Prasinophytes (24.85) > Cryptophytes(16.38).

5. Discussion

The thermal stress associated with the marine heatwave, as shown in the present study, reduced the primary productivity in the coastal water of the southern China. However, the main functional phytoplankton types showed resilience during the post-MHW recovery. This finding contrasted with the reported enhancement of primary productivity by MHW in the Mediterranean Sea (Soulie et al., 2023; Soulié et al., 2022). Such difference between the two regions might be due to different availability of nutrients and phytoplankton community structure (Huertas et al., 2011). It appears that MHW had positive under nutrient-rich but negative effects under nutrient-depleted conditions on phytoplankton (Hayashida et al., 2020; Sen Gupta et al., 2020).

The effects of MHWs can be assessed in two phases: thermal stress during the MHW and recovery following the thermal restoration to ambient temperature. The results of the warming phase with reduced primary productivity in this work were consistent with that of a land-based mesocosm experiment conducted at the Esplanad field station in Norway for about 3 weeks (Lassen et al., 2010). Another study showed that increasing temperature and light intensity both advanced the timing of bloom, but temperature had a greater effect on the phytoplankton community than light (Lewandowska and Sommer, 2010). In the present work, the MHW advanced the phytoplankton blooming by 2 days (Fig. 3). This is reasonable since subtropical marine photosynthesis increases with temperature rise from 15 to 24 °C (Gao et al., 2012; Mackey et al., 2013; Thomas et al., 2012). Nevertheless, extreme MHW can lead to species extinction and ecosystem collapse that may be difficult to recover (Garrabou et al., 2022; Suryan et al., 2021). The results that the mild MHW reduced primary productivity in the present study could be attributed to the initial blooming of the phytoplankton community triggered by the warming in April, which was also observed in other regions (Cahill et al., 2024).

Following the phytoplankton blooming, nutrient depletion and heat stress from day 5–9 (Figs. 1A and 2) led to a reduction in photosynthetic activity (Fig. 5), which was accompanied by decreased levels of carotenoids (Fig. 3B), indicating a diminished capacity for photoprotection under high solar radiation (Hayashida et al., 2020; Takaichi, 2011). Increased phytoplankton biomass led to the depletion of nutrients, which is responsible for the significant decrease in phytoplankton biomass and primary productivity in the later stages of the MHW (Figs. 3 and 4), which was also reported in other studies (Lewis et al., 2019; Malone et al., 1996). The assimilation number (C fixed per Chl *a* per time) appeared to remain unaffected by the MHW, even during the recovery phase (Fig. 4B). Therefore, the reduction in primary productivity (per volume of water) caused by the MHW should be attributed to decreased photosynthetic performance, specifically in terms of light use efficiency and high light tolerance. The increased NPQ during the post-MHW recovery period (Fig. 5D) indicates that the phytoplankton functional groups had gained the capacity to cope with high light stress (Lewis et al., 2019; Li et al., 2021; Qiao et al., 2021), which is positively correlated with the recovered primary productivity (Fig. 4B)(Lavaud et al., 2004).

In situ observations have shown that marine heatwaves alter the composition of phytoplankton communities (Arteaga and Rousseaux,

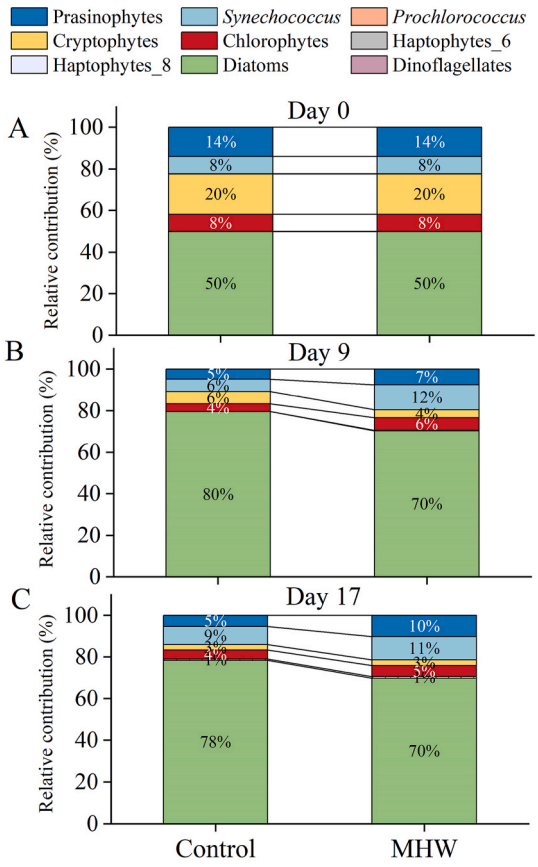

Fig. 6. | Taxonomic composition of phytoplankton assemblages of the coastal water (D0) and the waters in the control and heatwave groups at day 9 (end of HW treatment) and day 17 (end of the experiment). Percentage of different major phytoplankton groups are indicated in different colors on **(A)** Day 0, **(B)** Day 9, and **(C)** Day 17. Data are means ± SD of three replicates.

2023; Lewandowska and Sommer, 2010; Zhan et al., 2023). In this study, the MHW treatment inhibited the shift of the phytoplankton community to diatoms and slightly increased the percentage of Prasinophytes and *Synechococcus* (Fig. 6). A similar phenomenon was observed during the 2013 heatwave event in South Australia, where diatoms were the first to erupt and diminish, then transformed into other smaller planktonic species later (Roberts et al., 2019). Such phenomenon can be attributed to 1) the diatoms being less able to cope with the thermal stress and 2) the removal of nutrients aggravating the impact of MHW (Gao et al., 2000; Wang et al., 2006). It has been shown that the enzyme activity of nitrate reductase was reduced under elevated water temperature, leading to a decrease in the ability of large diatoms to utilize nitrate and subsequent inhibition of growth (Lomas and Glibert, 1999a, 1999b). On the other hand, smaller phytoplankton cells are considered to possess higher nutrient uptake and utilization efficiencies of nutrients, therefore, they are more likely to dominate the phytoplankton assemblages during the MHW period and post-MHW recovery period (Glibert et al., 2016).

The declined concentration of the macronutrients during the MHW period (Fig. 2A and D and Supplementary Fig. 2) appeared to have altered the proportions of the phytoplankton groups toward smaller ones (Fig. 6). The concentrations of NO_3^- and $Si(OH)_4$ increased during the recovery period (Fig. 2A and C). The MHW treatment could have led to faster dying off and enhanced remineralization (Supplementary Fig. 2), since higher seawater temperature facilitates the remineralization process of the dead cells, releasing large amounts of nutrients (Yamada and D'Elia, 1984) enhanced remineralization (Garber, 1984) and leading to the higher levels of nutrients (Fig. 2), therefore, resupply of nutrients should be responsible for the recovery of primary productivity (Fig. 4). It is most likely that the decrease in diatom proportion during and after the MHW treatment (D9-D11) might be due to the combined impacts of thermal stress and depletion of nutrients. However, the surges of NH_4^+ during and after the MHW in comparison to that of the control were unexpected. It might be related to ammonification driven by heterotrophic bacteria.

MHWs are suggested to alter phytoplankton communities to different extents in different waters (Feng et al., 2021; Wei et al., 2022a). For example, the Mediterranean heatwave in late spring/early summer in 2019 enhanced the abundance of diatoms, prymnesiophytes, and cyanobacteria but suppressed that of dinoflagellates (Soulié et al., 2022). In contrast, two consecutive heatwaves in the spring of 2022 in the Mediterranean Sea led to a shift in the phytoplankton community from diatom to cyanobacteria and chlorophytes (Soulie et al., 2023). Such differential impacts of MHW could be due to seasonal changes in chemical and physical environments. In the present study, the observed changes in phytoplankton community composition (Fig. 6) imply that marine food webs or microbial webs could be affected by MHW, since phytoplankton community changes are suggested to impact ecological and biogeochemical processes (Koch et al., 2014; Litchman et al., 2015). In this study, a decrease in the proportion of diatoms along with a reduced amount of biogenic silicon (Irion et al., 2021) may lead to a weakening of the 'bio-pump' effect and a reduction in the efficiency of carbon sequestration (Bopp et al., 2005; Tréguer et al., 2018).

After MHWs, some species may re-establish populations, thus contributing to biodiversity recovery (Ziegler et al., 2023). However, this depends on the resistance and resilience of phytoplankton populations and their interactions with abiotic and biotic conditions (Hillebrand et al., 2018). The observed resilience and recovery and notable temporal stability of the phytoplankton community in this study (Table 2) are inconsistent with the results from the mesoscale enclosure experiment that heatwave treatment lowered the resilience of some key functions in the Mediterranean Sea (Soulié et al., 2022). This is likely to be caused by the differences in multiple drivers, including nutrients, pH, CO_2, light, and other regional environmental traits, with nutrient concentration, local seawater temperature, and light intensity being particularly important (Soulie et al., 2023; Wei et al., 2022b).

6. Conclusion

In conclusion, the simulated marine heat waves in the spring season significantly reduced the biomass and primary productivity of phytoplankton communities in the coastal water of southern China. Nevertheless, the phytoplankton community and primary production could resume during the post-MHW period, showing notable resilience and tolerance related to primary productivity, phytoplankton functional

Table 2
| Average resistance, resilience, recovery, and temporal stability in terms of the daytime primary production (DPP) and phytoplankton functional types (PFTs).

	Average resistance (a)	Resilience (b)	Recover (c)	Temporal stability (d)
Function				
DPP	–	0.06	0.09	95.25
Chl *a*	−0.46	0.09	0.23	95.27
PFTs				
Diatoms	−1.09	0.13	−0.10	89.03
Chlorophytes	−0.50	0.09	0.22	85.81
Cryptophytes	−1.40	0.21	0.20	16.38
Synechococcus	−0.26	0.07	0.26	97.59
Prasinophytes	−0.51	0.15	0.68	24.85

All parameters in the table are calculated and evaluated according to the formulas in Table 1. In this experiment, function stability mainly included two aspects: daytime primary production (DPP) and Chl *a* (biomass), while compositional stability consisted of five aspects: Diatoms, Chlorophytes, Cryptophytes, *Synechococcus*, and Prasinophytes.

groups and photophysiology. Nevertheless, the reduced primary productivity by the MHW may lead to profound impacts on ecological processes and carbon cycles. Considering the impacts of multiple drivers (Boyd et al., 2018), the results of our work are limited to be extrapolated to understand the combined effects of MHW, ocean warming and acidification, which has been shown to alter phytoplankton community structure for both coastal and pelagic waters (Huang et al., 2021; Wei et al., 2021). Future simulated MHW experiments are expected to include changed levels of nutrients, pH, and solar UV radiation, and comparisons to field observations during and after *in situ* MHWs may further advance our understanding of MHW impacts in different regions and different seasons.

CRediT authorship contribution statement

Yukun Zhang: Writing – original draft, Investigation, Formal analysis, Data curation. **Guang Gao:** Writing – review & editing. **Huijie Xue:** Writing – review & editing, Methodology, Conceptualization. **Kunshan Gao:** Writing – review & editing, Writing – original draft, Supervision, Project administration, Methodology, Investigation, Funding acquisition.

Declaration of competing interest

The authors declare that they have no known competing financial interests or personal relationships that could have appeared to influence the work reported in this paper.

Acknowledgment

This study was supported by the National Key Research and Development Program (2022YFC3105303) and the National Natural Science Foundation of China (42361144840). The experiment was conducted in the Dongshan Swire Marine Station (D-SMART) of Xiamen University. We are grateful to the engineers, Xianglan Zeng and Wenyan Zhao for setting up the thermal controlling system, and to Mr. Shengyao Sun, Mr. Qisi Cai, Mr. Chichi Liu, Mr. Xuwen Fang, and all other staff and students working at the station for their logistic assistance during the experiment.

Appendix A. Supplementary data

Supplementary data to this article can be found online at https://doi.org/10.1016/j.envres.2024.120286.

Data availability

Data will be made available on request.

References

Arteaga, L.A., Rousseaux, C.S., 2023. Impact of Pacific Ocean heatwaves on phytoplankton community composition. Commun. Biol. 6, 263. https://doi.org/10.1038/s42003-023-04645-0.

Bopp, L., et al., 2005. Response of diatoms distribution to global warming and potential implications: a global model study. Gephys. Res. Lett. 32. https://doi.org/10.1029/2005GL023653.

Boyd, P.W., et al., 2018. Experimental strategies to assess the biological ramifications of multiple drivers of global ocean change—a review. Global Change Biol. 24, 2239–2261. https://doi.org/10.1111/gcb.14102.

Cahill, B., et al., 2024. Deconstructing co-occurring marine heatwave and phytoplankton bloom events in the Arkona Sea in 2018. Front. Mar. Sci. 11, 1323271. https://doi.org/10.3389/fmars.2024.1323271.

Carvalho, K., et al., 2021. Bering Sea marine heatwaves: patterns, trends and connections with the Arctic. J. Hydrol. 600, 126462. https://doi.org/10.1016/j.jhydrol.2021.126462.

Chatterjee, A., et al., 2022. Marine heatwaves in the Arabian Sea. Ocean Sci. 18, 639–657. https://doi.org/10.5194/os-18-639-2022.

Cheung, W.W., Frölicher, T.L., 2020. Marine heatwaves exacerbate climate change impacts for fisheries in the northeast Pacific. Sci. Rep. 10, 6678. https://doi.org/10.1038/s41598-020-63650-z.

Feng, Y., et al., 2021. The combined effects of increased pCO_2 and warming on a coastal phytoplankton assemblage: from species composition to sinking rate. Front. Mar. Sci. 8. https://doi.org/10.3389/fmars.2021.622319.

Frolicher, T.L., et al., 2018. Marine heatwaves under global warming. Nature 560, 360–364. https://doi.org/10.1038/s41586-018-0383-9.

Gao, G., et al., 2021. Impacts of marine heatwaves on algal structure and carbon sequestration in conjunction with ocean warming and acidification. Front. Mar. Sci. 8, 758651. https://doi.org/10.3389/fmars.2021.758651.

Gao, K., et al., 2012. Responses of marine primary producers to interactions between ocean acidification, solar radiation, and warming. Mar. Ecol. Prog. Ser. 470, 167–189. https://doi.org/10.3354/meps10043.

Gao, K., et al., 2007. Solar UV radiation drives CO_2 fixation in marine phytoplankton: a double-edged sword. Plant Physiol. 144, 54–59. https://doi.org/10.1104/pp.107.098491.

Gao, Y., et al., 2000. Temperature dependence of nitrate reductase activity in marine phytoplankton: biochemical analysis and ecological implications. J. Phycol. 36, 304–313. https://doi.org/10.1046/j.1529-8817.2000.99195.x.

Garber, J.H., 1984. Laboratory study of nitrogen and phosphorus remineralization during the decomposition of coastal plankton and seston. Estuar. Coast Shelf Sci. 18, 685–702. https://doi.org/10.1016/0272-7714(84)90039-8.

Garrabou, J., et al., 2022. Marine heatwaves drive recurrent mass mortalities in the Mediterranean Sea. Global Change Biol. 28, 5708–5725. https://doi.org/10.1111/gcb.16301.

Genty, B., et al., 1989. The relationship between the quantum yield of photosynthetic electron transport and quenching of chlorophyll fluorescence. Bba-Gen. Subjects. 990, 87–92. https://doi.org/10.1016/S0304-4165(89)80016-9.

Glibert, P.M., et al., 2016. Pluses and minuses of ammonium and nitrate uptake and assimilation by phytoplankton and implications for productivity and community composition, with emphasis on nitrogen-enriched conditions. Limnol. Oceanogr. 61, 165–197. https://doi.org/10.1002/lno.10203.

Hayashida, H., et al., 2020. Background nutrient concentration determines phytoplankton bloom response to marine heatwaves. Global Change Biol. 26, 4800–4811. https://doi.org/10.1111/gcb.15255.

Hillebrand, H., et al., 2018. Decomposing multiple dimensions of stability in global change experiments. Ecol. Lett. 21, 21–30. https://doi.org/10.1111/ele.12867.

Hobday, A.J., et al., 2016. A hierarchical approach to defining marine heatwaves. Prog. Oceanogr. 141, 227–238. https://doi.org/10.1016/j.pocean.2015.12.014.

Holbrook, N.J., et al., 2019. A global assessment of marine heatwaves and their drivers. Nat. Commun. 10, 2624. https://doi.org/10.1038/s41467-019-10206-z.

Hu, S., et al., 2020. Marine heatwaves in the Arctic region: variation in different ice covers. Gephys. Res. Lett. 47, e2020GL089329. https://doi.org/10.1029/2020GL089329.

Huang, R., et al., 2021. Elevated pCO_2 impedes succession of phytoplankton community from diatoms to dinoflagellates along with increased abundance of viruses and bacteria. Front. Mar. Sci. 8. https://doi.org/10.3389/fmars.2021.642208.

Huertas, I.E., et al., 2011. Warming will affect phytoplankton differently: evidence through a mechanistic approach. Proc. Biol. Sci. 278, 3534–3543. https://doi.org/10.1098/rspb.2011.0160.

Hughes, T.P., et al., 2017. Global warming and recurrent mass bleaching of corals. Nature 543, 373–377. https://doi.org/10.1038/nature21707.

Irion, S., et al., 2021. Small phytoplankton contribute greatly to CO_2-fixation after the diatom bloom in the Southern Ocean. ISME J. 15, 2509–2522. https://doi.org/10.1038/s41396-021-00915-z.

Koch, F., et al., 2014. Alteration of plankton communities and biogeochemical cycles by harmful Cochlodinium *polykrikoides* (Dinophyceae) blooms. Harmful Algae 33, 41–54. https://doi.org/10.1016/j.hal.2014.01.003.

Kweku, D.W., et al., 2018. Greenhouse effect: greenhouse gases and their impact on global warming. J. Sci. Res. Rep. 17, 1–9. https://doi.org/10.9734/JSRR/2017/39630.

Lassen, M.K., et al., 2010. The effects of temperature increases on a temperate phytoplankton community — a mesocosm climate change scenario. J. Exp. Mar. Biol. Ecol. 383, 79–88. https://doi.org/10.1016/j.jembe.2009.10.014.

Laufkötter, C., et al., 2020. High-impact marine heatwaves attributable to human-induced global warming. Science 369, 1621–1625. https://doi.org/10.1126/science.aba0690.

Lavaud, J., et al., 2004. General features of photoprotection by energy dissipation in planktonic diatoms (*Bacillariophyceae*) 1. J. Phycol. 40, 130–137. https://doi.org/10.1046/j.1529-8817.2004.03026.x.

Lewandowska, A., Sommer, U., 2010. Climate change and the spring bloom: a mesocosm study on the influence of light and temperature on phytoplankton and mesozooplankton. Mar. Ecol. Prog. Ser. 405, 101–111. https://doi.org/10.3354/meps08520.

Lewis, E., Wallace, D., 1998. Program developed for CO_2 system calculations. Environmental System Science Data Infrastructure for a Virtual Ecosystem (ESS-DIVE), United States, US Lawrence Berkely National Lab.

Lewis, K., et al., 2019. Photoacclimation of Arctic Ocean phytoplankton to shifting light and nutrient limitation. Limnol. Oceanogr. 64, 284–301. https://doi.org/10.1002/lno.11039.

Li, D., 1984. Geologic evolution of petroliferous basins on continental shelf of China. AAPG Bull. 68, 993–1003.

Li, Y., et al., 2022. The 2016 record-breaking marine heatwave in the Yellow Sea and associated atmospheric circulation anomalies. Atmos. Res. 268, 106011. https://doi.org/10.1016/j.atmosres.2021.106011.

Li, Z., et al., 2021. Nitrogen limitation decreases the repair capacity and enhances photoinhibition of photosystem II in a diatom. Photochem. Photobiol. 97, 745–752. https://doi.org/10.1111/php.13386.

Litchman, E., et al., 2015. Global biogeochemical impacts of phytoplankton: a trait-based perspective. J. Ecol. 103, 1384–1396. https://doi.org/10.1111/1365-2745.12438.
Lomas, M.W., Glibert, P.M., 1999a. Interactions between NH_4^+ and NO_3^- uptake and assimilation: comparison of diatoms and dinoflagellates at several growth temperatures. Mar. Biol. 133, 541–551. https://doi.org/10.1007/s002270050494.
Lomas, M.W., Glibert, P.M., 1999b. Temperature regulation of nitrate uptake: a novel hypothesis about nitrate uptake and reduction in cool-water diatoms. Limnol. Oceanogr. 44, 556–572. https://doi.org/10.4319/lo.1999.44.3.0556.
Mackey, K.R., et al., 2013. Effect of temperature on photosynthesis and growth in marine Synechococcus spp. Plant. Physiol. 163, 815–829. https://doi.org/10.1104/pp.113.221937.
Malone, T.C., et al., 1996. Scales of nutrient-limited phytoplankton productivity in Chesapeake Bay. Estuaries 19, 371–385.
Masson-Delmotte, V., et al., 2021. Climate change 2021: the physical science basis. Contribution of working group I to the sixth assessment report of the intergovernmental panel on climate change 2, 2391. https://doi.org/10.1017/9781009157896.001.
McCabe, R.M., et al., 2016. An unprecedented coastwide toxic algal bloom linked to anomalous ocean conditions. Gephys. Res. Lett . 43 (10), 366. https://doi.org/10.1002/2016GL070023, 10,376.
Mo, S., et al., 2022. Marine heatwaves impair the thermal refugia potential of marginal reefs in the northern South China Sea. Sci. Total Environ. 825, 154100. https://doi.org/10.1016/j.scitotenv.2022.154100.
Monteiro, M., et al., 2023. An emergent treat: marine heatwaves-Implications for marine decapod crustacean species-An overview. Environ. Res. 229, 116004. https://doi.org/10.1016/j.envres.2023.116004.
Oliver, E.C.J., et al., 2021. Marine heatwaves. Ann. Rev. Mar. Sci 13, 313–342. https://doi.org/10.1146/annurev-marine-032720-095144.
Oliver, E.C.J., et al., 2018. Longer and more frequent marine heatwaves over the past century. Nat. Commun. 9, 1324. https://doi.org/10.1038/s41467-018-03732-9.
Perkins-Kirkpatrick, S., et al., 2016. Natural hazards in Australia: heatwaves. Clim. Change 139, 101–114. https://doi.org/10.1007/s10584-016-1650-0.
Qiao, H., et al., 2021. Physiological responses of the diatoms *Thalassiosira weissflogii* and *Thalassiosira pseudonana* to nitrogen starvation and high light. Mar. Environ. Res. 166, 105276. https://doi.org/10.1016/j.marenvres.2021.105276.
Ritchie, R.J., 2006. Consistent sets of spectrophotometric chlorophyll equations for acetone, methanol and ethanol solvents. Photosynth. Res. 89, 27–41. https://doi.org/10.1007/s11120-006-9065-9.
Roberts, S.D., et al., 2019. Marine heatwave, harmful algae blooms and an extensive fish kill event during 2013 in South Australia. Front. Mar. Sci. 6. https://doi.org/10.3389/fmars.2019.00610.
Sakshaug, E., et al., 2009. Phytoplankton and Primary Production. Ecosystem Barents Sea, pp. 167–208.
Scannell, H.A., et al., 2016. Frequency of marine heatwaves in the North Atlantic and North Pacific since 1950. Gephys. Res. Lett . 43, 2069–2076. https://doi.org/10.1002/2015GL067308.
Sen Gupta, A., et al., 2020. Drivers and impacts of the most extreme marine heatwave events. Sci. Rep. 10, 19359. https://doi.org/10.1038/s41598-020-75445-3.
Smale, D.A., et al., 2019. Marine heatwaves threaten global biodiversity and the provision of ecosystem services. Nat. Clim. Change 9, 306–312. https://doi.org/10.1038/s41558-019-0412-1.
Smith, K.E., et al., 2023. Biological impacts of marine heatwaves. Ann. Rev. Mar. Sci 15, 119–145. https://doi.org/10.1146/annurev-marine-032122-121437.
Soulie, T., et al., 2023. Functional and structural responses of plankton communities toward consecutive experimental heatwaves in Mediterranean coastal waters. Sci. Rep. 13, 8050. https://doi.org/10.1038/s41598-023-35311-4.
Soulié, T., et al., 2022. Functional stability of a coastal mediterranean plankton community during an experimental marine heatwave. Front. Mar. Sci. 9. https://doi.org/10.3389/fmars.2022.831496.
Suryan, R.M., et al., 2021. Ecosystem response persists after a prolonged marine heatwave. Sci. Rep. 11, 6235. https://doi.org/10.1038/s41598-021-83818-5.
Takaichi, S., 2011. Carotenoids in algae: distributions, biosyntheses and functions. Mar. Drugs 9, 1101–1118. https://doi.org/10.3390/md9061101.
Tan, H.-J., et al., 2023. Causes of 2022 summer marine heatwave in the East China Seas. Adv. Clim. Change Res. 14, 633–641. https://doi.org/10.1016/j.accre.2023.08.010.
Thomas, M.K., et al., 2012. A global pattern of thermal adaptation in marine phytoplankton. Science 338, 1085–1088. https://doi.org/10.1126/science.1224836.
Tréguer, P., et al., 2018. Influence of diatom diversity on the ocean biological carbon pump. Nat. Geosci. 11, 27–37. https://doi.org/10.1038/s41561-017-0028-x.
Vallina, S.M., et al., 2014. Global relationship between phytoplankton diversity and productivity in the ocean. Nat. Commun. 5, 4299. https://doi.org/10.1038/ncomms5299.
Wang, L., et al., 2015. The modification and optimizing of the CHEMTAX running in the South China Sea. Hai Yang Xue Bao 34, 124–131. https://doi.org/10.1007/s13131-015-0621-z.
Wang, Z., et al., 2006. Study on population growth processes and interspecific competition of Prorocentrum donghaiense and Skeletonema costatum in semi-continuous dilution experiments. Adv. Mar. Biol. 24, 495. https://api.semanticscholar.org/CorpusID:88083292.
Wei, Y., et al., 2022a. Different responses of phytoplankton and zooplankton communities to current changing coastal environments. Environ. Res. 215, 114426. https://doi.org/10.1016/j.envres.2022.114426.
Wei, Y., et al., 2022b. Exploring the dynamics of marine picophytoplankton among the Yellow Sea, Indian Ocean and Pacific Ocean: the importance of temperature and nitrogen. Environ. Res. 214, 113870. https://doi.org/10.1016/j.envres.2022.113870.
Wei, Y., et al., 2021. Phosphorus enrichment masked the negative effects of ocean acidification on picophytoplankton and photosynthetic performance in the oligotrophic Indian Ocean. Ecol. Indicat. 125. https://doi.org/10.1016/j.ecolind.2021.107459.
Wong, G.T., et al., 2015. The oceanography of the northern South China Sea Shelf-Sea (NoSoCS) and its adjacent waters—overview and highlights. Deep-sea. Res. Pt. II 117, 3–9. https://doi.org/10.1016/j.dsr2.2015.04.026.
Wu, L., et al., 2012. Enhanced warming over the global subtropical western boundary currents. Nat. Clim. Change 2, 161–166. https://doi.org/10.1038/NCLIMATE1353.
Xiao, W., et al., 2018. Realized niches explain spatial gradients in seasonal abundance of phytoplankton groups in the South China Sea. Prog. Oceanogr. 162, 223–239. https://doi.org/10.1016/j.pocean.2018.03.008.
Yamada, S.S., D'Elia, C.F., 1984. Silicic acid regeneration from estuarine sediment cores. Mar. Ecol. Prog. Ser. Oldendorf. 18, 113–118.
Yao, Y., Wang, C., 2021. Variations in summer marine heatwaves in the South China Sea. J. Geophys. Res-Oceans 126, e2021JC017792. https://doi.org/10.1029/2021JC017792.
Yao, Y., et al., 2020. Marine heatwaves in China's marginal seas and adjacent offshore waters: past, present, and future. J. Geophys. Res-Oceans 125, e2019JC015801. https://doi.org/10.1029/2019JC015801.
Zhan, W., et al., 2023. Shifting responses of phytoplankton to atmospheric and oceanic forcing in a prolonged marine heatwave. Limnol. Oceanogr. 68, 1821–1834. https://doi.org/10.1002/lno.12388.
Ziegler, S.L., et al., 2023. Marine protected areas, marine heatwaves, and the resilience of nearshore fish communities. Sci. Rep. 13, 1405. https://doi.org/10.1038/s41598-023-28507-1.